ADVANCES IN ATMOSPHERIC SCIENCES, VOL. 40, MAY 2023, 804–823

• Original Paper •

The Initial Mesoscale Vortexes Leading to the Formation of Tropical Cyclones in the Western North Pacific※

Shenglan WU[1,2] and Juan FANG*[2]

[1]*Shanghai Central Meteorological Observatory*, *CMA*, *Shanghai* 200030, *China*

[2]*Key Laboratory of Mesoscale Severe Weather (MOE)*, *School of the Atmospheric Sciences*, *Nanjing University*, 163 *Xianlin Road*, *Nanjing* 210046, *China*

(Received 8 February 2022; revised 5 July 2022; accepted 22 August 2022)

ABSTRACT

A statistical analysis of the initial vortexes leading to tropical cyclone (TC) formation in the western North Pacific (WNP) is conducted with the ECMWF ERA5 reanalysis data from 1999 to 2018. It is found that TCs in the WNP basically originate from three kinds of vortexes, i.e., a mid-level vortex (MV), a low-level vortex (LV), and a relatively deep vortex with notable vorticity in both the lower and middle troposphere (DV). Among them, LV and DV account for 47.9% and 24.2% of tropical cyclogenesis events, respectively, while only 27.9% of TCs develop from the MV, which is much lower than that which occurs in the North Atlantic and eastern Pacific. Such a difference might be ascribed to the active monsoon systems in the WNP all year round. Due to the nearly upright structure of mid-level convergence in the early pre-genesis stage, TC genesis efficiency is the highest in DV. Compared with MV, LV generally takes a shorter time to intensify to a TC because of the higher humidity and the stronger low-level cyclonic circulation, which is related to air-sea interaction and boundary-layer convergence. Further examination of the relationship between tropical cyclogenesis and large-scale flow patterns indicate that the TC genesis events associated with LV are primarily related to the monsoon shear line, monsoon confluence region, and monsoon gyre, while those associated with MV are frequently connected with easterly waves and wave energy dispersion of preexisting TC. Compared with other flow patterns, tropical cyclones usually form and intensify faster in the monsoon confluence region.

Key words: TC formation, initial mesoscale vortexes, TC genesis efficiency, large-scale flow patterns

Citation: Wu, S. L., and J. Fang, 2023: The initial mesoscale vortexes leading to the formation of tropical cyclones in the western North Pacific. *Adv. Atmos. Sci.*, **40**(5), 804–823, https://doi.org/10.1007/s00376-022-2029-y.

Article Highlights:

- TCs in the WNP originate from three archetypes of vortexes, i.e., mid-level vortex, low-level vortex, and relatively deeper vortex.
- Most of the TCs originate from LV-type, while 27.9% and 24.2% of the TCs develop from MV-type and DV-type, respectively.
- TC genesis events associated with LV are primarily related to SL, CR, and GY, while MV are frequently connected with EW and PTC.

1. Introduction

Understanding tropical cyclone (TC) formation and evolution under complex multiscale processes is fundamental to improve TC forecasts and emergency response plans. The large-scale conditions favorable for TC formation have been well known, namely, deep thermocline with sea-surface temperature higher than 26.5°C, weak vertical wind shear, cyclonic low-level vorticity, organized deep moist convection, sufficient amount of moisture, and a warm core in the middle troposphere (Gray, 1968; Briegel and Frank, 1997). However, the infrequent and sporadic formation of TCs within regions having favorable large-scale conditions indicates that mesoscale processes, such as a mesoscale cyclonic vortex or vortical hot towers, play key roles in tropical cyclogenesis (Holland, 1995; Bister and Emanuel, 1997; Ritchie and Holland, 1997; Montgomery et al., 2006). To date, the mesoscale systems controlling the formation of a

※ This paper is a contribution to the special issue on the 14th International Conference on Mesoscale Convective Systems and High-Impact Weather.

* Corresponding author: Juan FANG
Email: fangjuan@nju.edu.cn

TC are still not clear and are the focus of ongoing research. There are many unsolved and debatable issues about the mesoscale dynamical processes leading to TC formation. One of the issues concerns which kind of mesoscale vortex can result in a well-organized TC vortex leading to tropical cyclogenesis.

The midtropospheric mesoscale cyclonic vortex customarily develops within a mesoscale convective system (MCS) or mesoscale convective complex, and it is a very common feature in the tropics. Some observational studies show that such a mesoscale vortex usually precedes the tropical cyclogenesis (e.g., Simpson et al., 1997; Raymond et al., 2011; Komaromi, 2013; Zawislak and Zipser, 2014). From the perspective of vortex dynamics, Ritchie and Holland (1997) and Bister and Emanuel (1997) described the possible roles of the midlevel mesoscale cyclonic vortex in the TC formation. The former suggested that the merger of the mid-level vorticity anomalies in the MCSs will result in a large mid-level mesoscale cyclonic vortex with deep penetration depth, which can induce the strengthening of low-level cyclonic circulation. By contrast, Bister and Emanuel (1997) found that the downward extension of the mid-level cyclonic vortex via vertical advection can spin-up the TC surface circulation.

Considering that the midlevel mesoscale cyclonic vortex is usually coupled with a low-level cold anomaly, Raymond et al. (2014) argued that the relative humidity is usually high under the mid-level vortex, which greatly aids the development of deep convection and spin-up of a TC by weakening the evaporative cooling and the downward mass flux in the lower troposphere. Different from Raymond et al. (2014), Dunkerton et al. (2009) proposed the "marsupial paradigm" to illuminate the influence of midlevel mesoscale cyclonic vortex on the convective activity and TC formation. They suggested that the closed circulation of the mid-level vortex can serve as a wave-pouch (a region of closed circulation in the co-moving frame of reference) to protect the deep convection from dry air intrusion and vertical wind shear, favoring sustained deep convection inside the vortex and then TC formation. Dunkerton et al. (2009) further pointed out that approximately 90% (55 out of 61 tropical storms and hurricanes) of tropical cyclogenesis events in the North Atlantic and eastern Pacific from 2000 to 2001 were associated with the wave pouch theory. In the western North Pacific (WNP), Zhang et al. (2010) and Guo and Zhang (2012) also found that the mid-level cyclonic vortex made important contributions to the formation of Typhoon Durian (2001). Zhang et al. (2010) indicated that the mesoscale vortex plays multiple roles of organizing the system, maintaining vorticity memory, and providing for vertical uniformity. Guo and Zhang (2012) emphasized that the merger of mesoscale vortexes may be a possible inducing mechanism for the tropical cyclogenesis.

In addition to the mid-level vortex, the low-level vortex sometimes can also be the precursor of a TC. Davis and Bosart (2004) showed that during the formation of Hurricane Humberto (2001), rather than a traceable downward extension of a mid-level vortex, the low-level vorticity became noticeable and the initial vorticity enhancement occurred over a relatively shallow layer with peak vorticity centered at about z = 1–2 km. Through a cloud-resolving simulation, Fang and Zhang (2010) suggested that the surface-based vortex of incipient TC Dolly (2008) and the formation of cold pools at low levels first appeared after the burst of convection. Furthermore, according to Wu and Fang (2019), Super Typhoon Nepartak (2016) originated from an embedded low-level vorticity perturbation due to the breakdown of the intertropical convergence zone (ITCZ) over the WNP.

The concentration of humidity and stretching associated with the low-level cyclonic circulation is conducive to the outbreak of deep convection and the development of small-scale vortical hot towers (VHTs). The coalescence and growth of deep convective VHTs subtract energy from the ocean and release latent heat to moisten the troposphere, accelerating the spin-up of the surface vortex and engendering the nascent TC through the upward transport of low-level cyclonic vorticity connected with deep convection (Montgomery and Enagonio, 1998; Möller and Montgomery, 2000; Hendricks et al., 2004; Montgomery et al., 2006; Tory et al., 2006a, b).

Because the above mentioned two archetypes represent end points on the spectrum of precursors, we do not anticipate that there is a clear threshold separating one type from another. In fact, the vorticity anomalies are sometimes spatially distinct in both the lower and middle troposphere during the early pre-genesis stage of TCs. Based on numerical simulation and theoretical analysis, Zhang et al. (2021) investigated the characteristics and mechanism of vertical vortexes coupling in the genesis of TC Durian (2001) over the South China Sea and emphasized the importance of VHTs in coupling the initial vortexes in the low- and mid-levels until the vortex system developed sufficient amplitude due to wind-induced surface heat exchange (WISHE) instability (Emanuel, 1994).

Up to now, studies of the mesoscale processes leading to TC formation primarily concentrated on the North Atlantic and eastern Pacific basins, yet the WNP is the region with the most TCs globally. Due to the active Asian monsoon, the large-scale background circulations of tropical cyclogenesis are much more complex in the WNP than that in the North Atlantic and eastern Pacific basins. Holland (1995) considered the major components of monsoon circulation in the WNP to be monsoon depression, westerly monsoonal flow, and confluence zone to the east of the monsoon. Via the Japanese Geostationary Meteorological Satellite (GMS) and an 8-yr analysis set, Ritchie and Holland (1999, hereafter RH99) broadened and extended the early work of Holland (1995) and classified the major flow patterns preferring TC genesis in the WNP into five categories: monsoon shear line (SL), monsoon confluence region (CR), monsoon gyre (GY), easterly wave (EW), and wave energy dispersion of preexisting TC (PTC). It remains uncertain whether the TC originates from different mesoscale processes under different large-scale flow patterns. However, such an issue has not been discussed in the literature.

To deepen the understanding of mesoscale features and processes of tropical cyclogenesis, a statistical analysis on TC formation in the WNP is performed in this work with focus on the role of mesoscale vortices in the tropical cyclogenesis and their relationship with the large-scale background circulation. The rest of the paper is organized as follows. Section 2 introduces the data and analysis method. Section 3 overviews the statistical characteristics and the large-scale environmental circulations of three archetypes of TC genesis in WNP. The genesis efficiency of TC genesis associated with different mesoscale vortexes is also presented in section 3. Section 4 and 5 provide the discussion and concluding remarks.

2. Data and methodology

The analyses in this study are based on the European Centre for Medium-Range Weather Forecasts (ECMWF) fifth-generation global atmospheric reanalysis (ERA5) at 0.25° resolution every 6 hours from 1999 to 2018. The tropical cyclogenesis records are taken from the Joint Typhoon Warning Center (JTWC) best-track data (Chu et al., 2002) in the WNP basin and the time of TC genesis is defined as when the first tropical depression (TD) record appears in the JTWC best-track dataset following DeMaria et al., (2001), e. g. the maximum sustained surface winds greater than 25 kt. Among the 580 best-track records in the WNP basin over 20 years, 42 records indicating the TC formed east of 165°E or north of 30°N are excluded following RH99. Therefore, there are a total of 538 records employed in this study.

2.1. *Identification of the initial vortex leading to tropical cyclogenesis*

The identification of the initial vortex leading to tropical cyclogenesis relies on detecting and tracking the vortex centers before TC formation. Following Hodges (1994, 1995, 1999), the pre-TC disturbance was tracked before tropical cyclogenesis with filtered relative vorticity at the level of 1000 and 600 hPa. Here, we choose constant pressure levels of 1000- and 600-hPa to represent the lower and middle troposphere. First, the vorticity field was spectrally filtered using Gaussian smoothing with a standard deviation of 1 degree within a domain of 2000 km to eliminate the local vorticity maximum caused by local convection so that the track trajectories would be smoother and more successive. The tracking algorithm was realized by detecting the vorticity maxima that exceed a threshold of 1.5×10^{-5} s^{-1} using the steepest ascent maximization method (Hodges, 1995). Then the vorticity maxima of adjacent times were preliminarily linked together by applying a nearest-neighbor approach and finally refined by a B-spline interpolation and minimizing a cost function for track smoothness (Hodges, 1999, Hodges et al., 2017). A distance check between two sequential times at one special layer was performed to help ensure that the tracker found did not exceed a specific distance and belonged to the same system. When distance became too large, the tracker would terminate tracking for this particular disturbance. The distance threshold was set as 330 km for current study. One example of vortex tracking is shown in Fig. 1. Figure 1a shows the relative vorticity at 1000 hPa in WNP at a specific time, and Fig. 1b is the filtered vorticity after Gaussian smoothing. The green dots represent the vorticity maxima exceeding a threshold of 1.5×10^{-5} s^{-1} detectable at this specific time, and the black dots are the location of the past or the future of these vorticity maxima, connected by black lines with a nearest-neighbor approach. The track we can see is the final state after being refined by a B-spline interpolation and minimizing a cost function for track smoothness.

The initial vortex leading to tropical cyclogenesis was identified according to the longevity of vortex tracking in the lower and middle troposphere, which is defined as the period from the time when the vorticity exceeds the threshold that can be detected to the TC genesis moment. If the 1000-hPa (600-hPa) vorticity anomaly could be tracked for a longer time compared with the 600-hPa (1000-hPa) vorticity anomaly, then the genesis is assumed to have resulted from a low-level (mid-level) vorticity anomaly. When the difference between the tracking periods of 1000- and 600-hPa vorticity anomalies is less than or equal to 6 hours, the genesis event is taken as resulting from both low-level and mid-level vorticity anomalies, so it is thought to be induced by a relatively deep vortex in the lower-to-middle troposphere. For brevity, the archetypes of TC genesis mentioned above are respectively referred to as LV-type, MV-type, and DV-type hereafter.

2.2. *Identification of major environmental flow patterns*

Using the subjective classification procedure, RH99 categorized the environmental circulation preferred for tropical cyclogenesis into five large-scale dynamical patterns in the WNP, i.e., SL, CR, GY, EW, and PTC. Based on this, Yoshida and Ishikawa (2013, hereafter YI13) developed an objective algorithm for computing "scores" to classify major flow patterns favoring TC formation over the WNP, in which the contribution to the TC formation from each large-scale flow pattern is quantitatively denoted by a score calculated from the reanalysis data. The "contribution scores" consist of an intensity term and a distance term, and they are normalized by their maximum values so they can be compared to that of the other flow patterns (contribution scores in Fig. 2). They are calculated based on the zonal and meridional wind components at 850 hPa, as well as the sea level pressure.

In order to reduce the influence of some high-frequency disturbances and try to unify the "contribution scores" so that they can be compared with other flow patterns more acceptable, an objective detection method was employed in this work with some modifications. First, the TC-related signals were removed from the ERA5 wind field following the procedure proposed by Kurihara et al. (1993, 1995) before the calculation of contribution scores related to the SL, CR, GY, and EW patterns. The elimination of TC signals can largely avoid the occurrence of a false high score for SL or

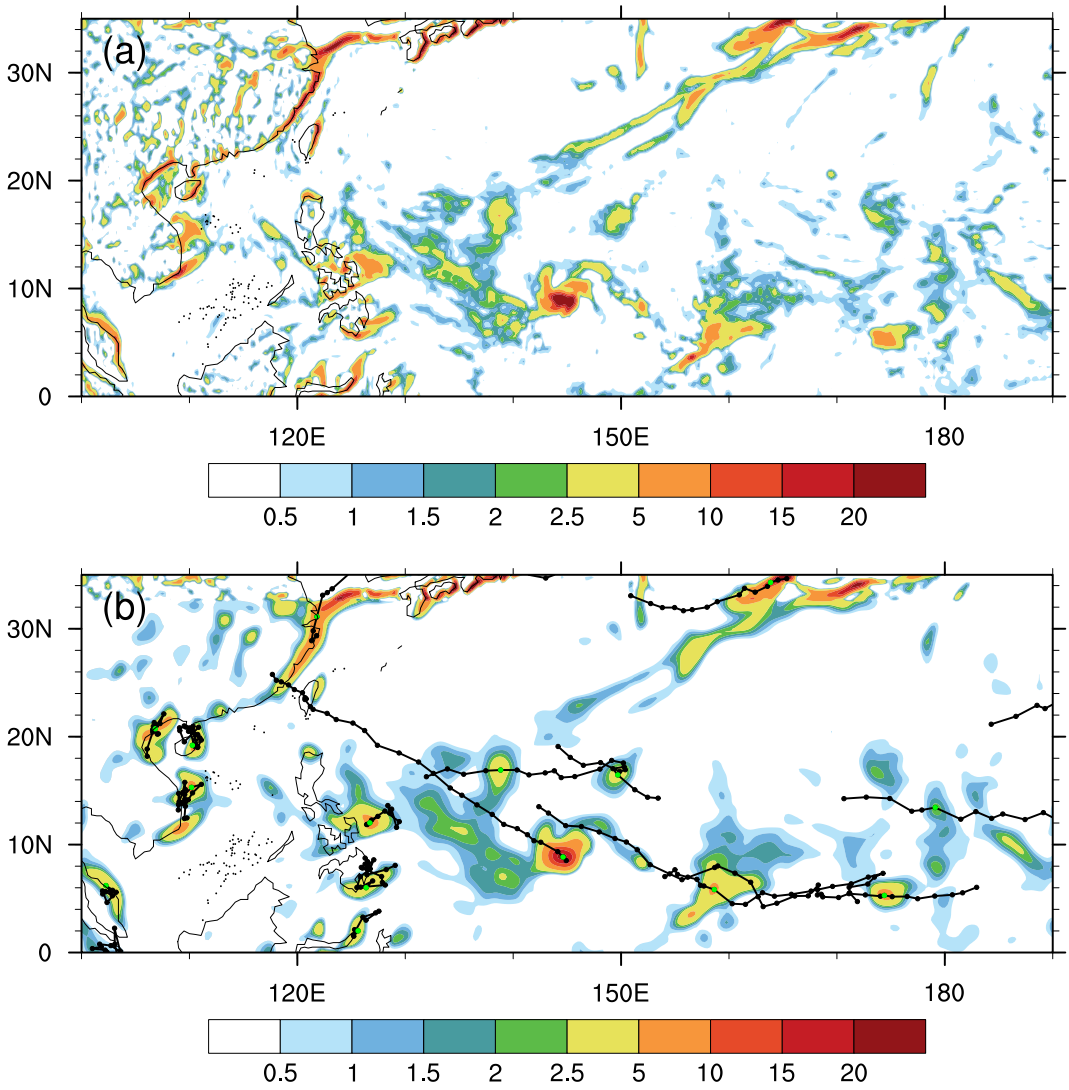

Fig. 1. Example of vortex tracking: (a) 1000-hPa relative vorticity (units: 10^{-5} s^{-1}) at 0000 UTC 3 July 2016. (b) Filtered vorticity (units: 10^{-5} s^{-1}) and tracking trajectories.

CR. Second, a low-pass Lanczos filter with a 10-day cutoff period was applied to the wind fields before the calculation of contribution scores related to the SL, CR, and GY patterns (Duchon, 1979; preconditioning in Fig. 2). Finally, the contribution score of GY was derived from a new algorithm on the basis of Wu et al. (2013, hereafter W13), i.e.,

$$\mathrm{SCR_{GY}} = \frac{\oint_S \boldsymbol{V}\cdot\delta\boldsymbol{r}\cdot\exp(A\times d_{\mathrm{ist}})}{\mathrm{Max}\,[\mathrm{SCR_{GY}}]},$$

where $\oint_S \boldsymbol{V}\cdot\delta\boldsymbol{r}$ is the relative circulation on the gyre center within a radius of 10°. The gyre center is searched within a test domain, the length and the width of which are both 15 grid cells centered at the tropical cyclogenesis location, and defined as the location where it is surrounded by cyclonic circulation that has an outermost closed isobar with a diameter on the order of 2200 km (Lander, 1994; Harr et al., 1996). In Eq. (1), the parameter d_{ist} represents the distance between the TC genesis location and the gyre center, and A is a tuning parameter to adjust the distance range for the exponential function that is empirically set to -2.0×10^{-7}. The contribution score is normalized by its maximum value, Max[$\mathrm{SCR_{GY}}$], following other flow patterns in YI13. RH99 suggested that the GY is quite different from the SL since the former has lower sea level pressure in a larger region, so the GY score was calculated only for cases when the central minimum sea level pressure was lower than 1006 hPa (Fig. 12 in RH99). For the GY pattern, the filtered 850-hPa wind and the sea level pressure at the TC genesis time were adopted because the cyclonic circulation in the GY pattern is more significant than that in the SL and CR patterns at the TC genesis time (RH99; time selection in Fig. 2).

RH99 and Zehr (1992) suggested that the TC perturbation usually occurs approximately 72 h prior to the TC genesis time. Briegel and Frank (1997) also indicated that the southwesterly surges related to SL and CR appear at around 72 h before TC genesis in the WNP. Based on these studies, YI13 derived the "contribution scores" of the SL, CR, and

EW flow patterns from the averaged 850-hPa wind field at 66 and 72 h before the TC genesis time. In our work, the "contribution score" of PTC pattern was also computed with the ERA5 data at 69 h prior to the TC genesis time because the appearance of a preexisting TC in the northwest quadrant 72 h prior to TC genesis is necessary to define the PTC pattern (RH99; time selection in Fig. 2). In practice, the PTC pattern derived from ERA5 69 h before genesis is much more reliable than that at the TC genesis time, even though the wave train in the PTC pattern is more remarkable at the TC genesis time (YI13).

Table 1 shows the number and percentage of five large-scale flow patterns associated with tropical cyclogenesis in the WNP during the period from 1999 to 2018. Among the 538 TCs, the most frequent flow pattern is SL (37.0% of the total), followed by EW (18.6%) and CR (17.7%). PTC and GY patterns account for 13.9% and 12.8%, respectively. As we can see, there is no unclassified flow pattern as in YI13. If cases existed with no value for the scores of any of the five patterns, the valid time of 850-hPa wind used to compute the contribution scores was adjusted according to the tracking longevity of the vortex case by case.

The statistical results of the large-scale flow patterns in the current study were compared with YI13, RH99, W13, and Zong and Wu (2015, hereafter ZW15), which are all conducted in the WNP but during different periods (Table 1). In all analyses, SL is the most frequent pattern (also in ZW15, which combined SL and CR together into the monsoon trough), followed by EW and CR at approximately 20%, whereas PTC and GY have small frequencies. Since we put forward a new algorithm to calculate the contribution score of GY following W13, it is necessary to discuss some main

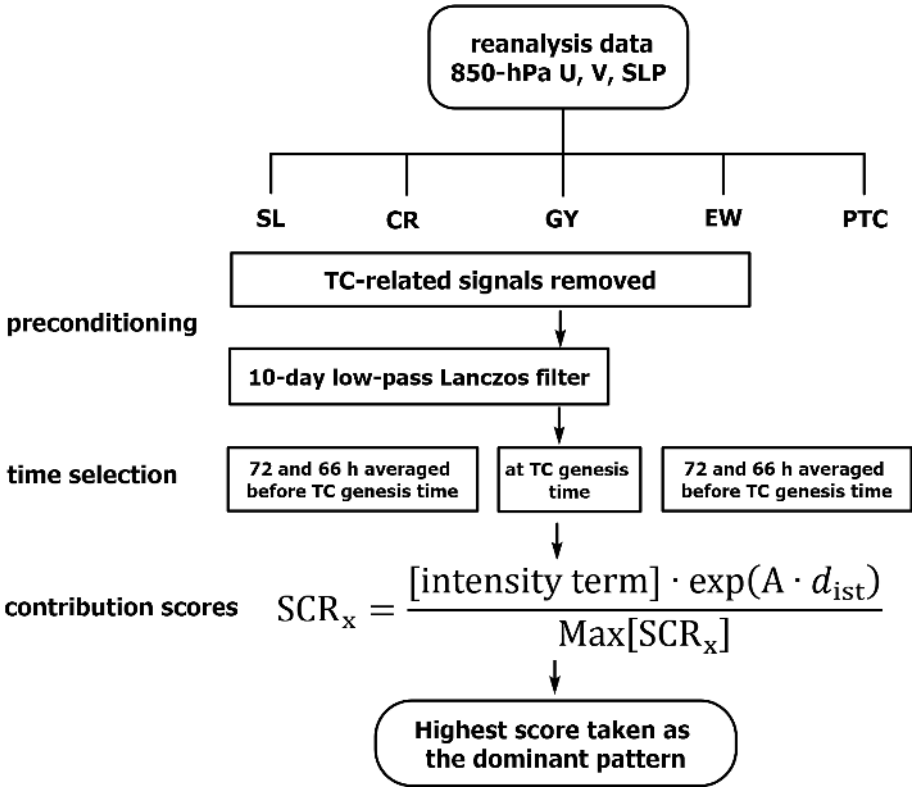

Fig. 2. Flowchart describing the classification algorithm of major environmental flow patterns.

Table 1. Statistical summary of five large-scale flow patterns associated with TC genesis in the WNP for the 20-yr study period from 1999 to 2018 and categorization results in YI13, RH99, W13, and ZW15. SL, CR, GY, EW, and PTC stand for the monsoon shear line, monsoon confluence region, monsoon gyre, easterly waves, and wave energy dispersion of preexisting TC, respectively. The percent in parentheses represents the proportion of each flow pattern.

	ALL	SL	CR	GY	EW	PTC
Current (1999–2018)	538	199 (37.0%)	95 (17.7%)	69 (12.8%)	100 (18.6%)	75 (13.9%)
YI13 (1979–2008)	908	380 (41.9%)	146 (16.1%)	59 (6.5%)	165 (18.2%)	97 (10.7%)
RH99 (1984–92)[1]	199	84 (42.2%)	58 (29.1%)	5 (2.5%)	36 (18.1%)	16 (8.0%)
W13 and ZW15 (2000–10)[2]	212	91 (43.1%)		42 (19.8%)	–	–

[1]1989 is excluded.
[2]Only May–October are considered.

reasons that cause the percentage discrepancy of the GY pattern with that in W13. Actually, W13 analyzed only the tropical cyclogenesis associated with monsoon gyres and did not consider the PTC and EW patterns at the same time, while many tropical cyclogenesis cases were influenced by two or more environmental flow patterns simultaneously. Under this kind of situation, we need to compute the contribution scores from different patterns to determine the dominant one. Therefore, in our current study, not all tropical cyclogenesis under the influence of monsoon gyre is categorized into the GY pattern.

Figure 3 displays the composite large-scale circulation of the five flow patterns at the first time when the initial mesoscale vortex is detected. We can see there are some major differences among different flow patterns. The shear line and confluence region of SL and CR occur preferentially equatorward (around 5°–10°N), in keeping with the break of ITCZ and the monsoon trough (Figs. 3b–c). Compared with SL and CR, GY appears poleward (around 15°–20°N) and westward, and the cyclonic circulation is obvious (Fig. 3d). Such features are much more evident at the TC genesis time (not shown). The EW pattern is dominated by broad easterly flow (Fig. 3e). The large-scale circulation of PTC is quite close to that of the GY pattern with distinct cyclonic circulation (Fig. 3f). The major differences among these five typical large-scale circulation systems further illustrate the effectiveness and validity of environmental flow patterns classification algorithm.

3. Statistical characteristics of the three archetypes of TC genesis in WNP

3.1. *The statistics of three archetypes of TC genesis*

From Table 2, we can see that most of the TCs originated from the low-level vortex (47.9%) while 27.9% and 24.2%

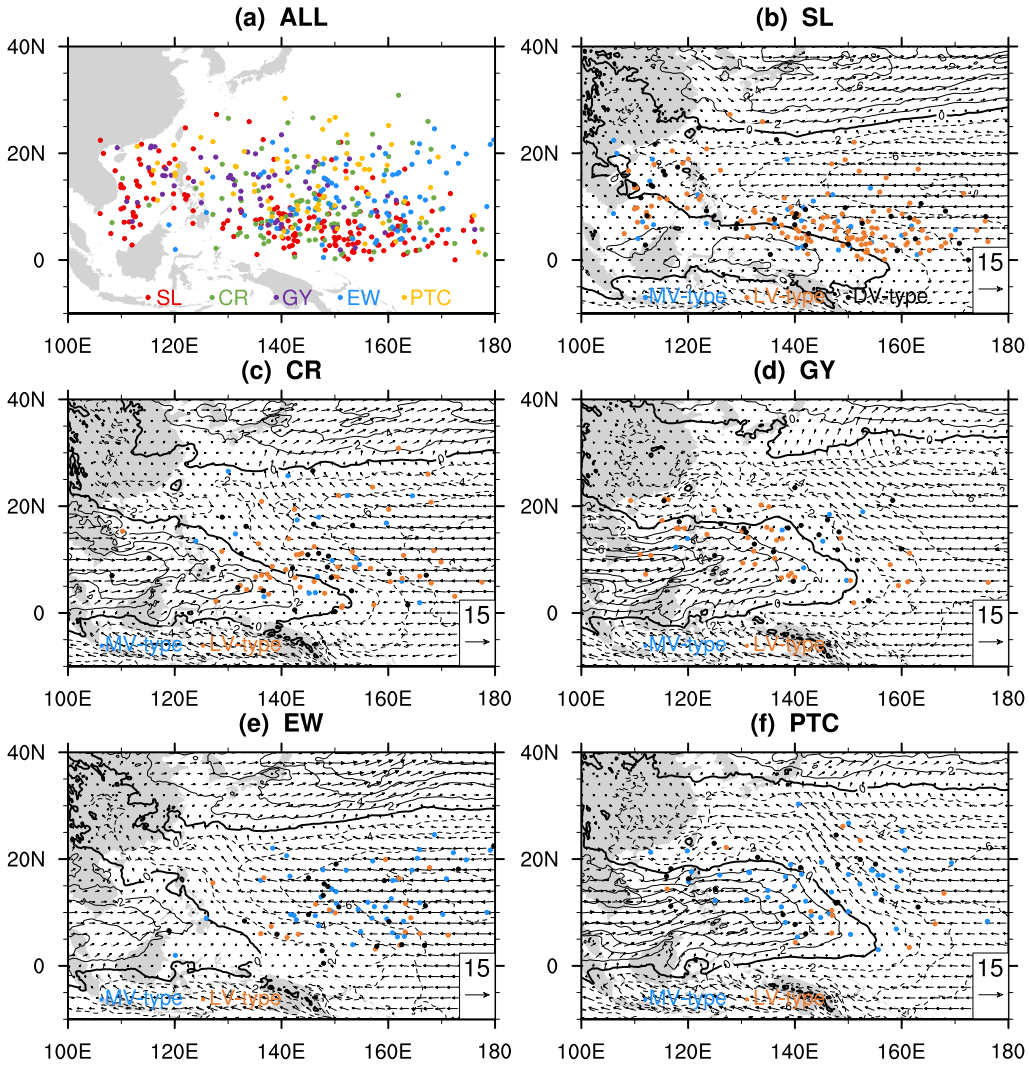

Fig. 3. The origin of vortex perturbation (the first time when initial vortex can be detected) for (a) all analyzed TCs in WNP and for (b)–(f) three archetypes of TC genesis in the five large-scale background flow patterns. Vectors are the composite 850-hPa wind field (units: m s^{-1}) at the time when pre-TCs first appear, and the contour is the zonal wind (units: m s^{-1}) at the same height.

of the TCs developed from the mid-level vortex and deep vortex, respectively, over the WNP in the period of 1999–2018. The proportion of MV-type tropical cyclogenesis in the WNP is much lower than that in the North Atlantic and eastern Pacific, where about 90% of TCs developed under the protection of a "wave pouch" in the mid-troposphere (Dunkerton et al., 2009). Such a difference might be ascribed to the following two reasons. On the one hand, Dunkerton et al. (2009) only focused on the mid-level vortex during TC formation, but in fact, the mid-level vorticity anomalies can also be generated in the TC genesis events associated with LV and DV. On the other hand, the large-scale background circulations of tropical cyclogenesis in WNP are usually associated with the East Asian monsoon system, which is different from the North Atlantic and eastern Pacific basins in that they are influenced by easterly waves all year round. The large-scale background flow pattern of the monsoon trough makes it relatively easier for a low-level disturbance to develop much faster in WNP. Moreover, from the classification results of initial vortexes leading to tropical cyclogenesis, we should note that a substantial part of TCs with a relatively deep vortex develop simultaneously in the lower and middle troposphere, which is often ignored in previous work.

Seasonal variation in the proportion of different archetypes of TC genesis is displayed in Fig. 4. From Figs. 4a–b we can see that three types of initial vortexes leading to TC genesis occur in all months and the seasonal changes are not apparent. From around July to October, the percentage of the LV-type decreases while the MV-type and

Table 2. Statistical summary of archetypes of TC genesis and five large-scale flow patterns in the WNP from 1999 to 2018. MV, LV, and DV stand for the mid-level vortex, low-level vortex, and relatively deep vortex leading to TC genesis. The percent in parentheses represents the proportion of each archetype of TC genesis and flow pattern.

	ALL	SL	CR	GY	EW	PTC
ALL	538	199 (37.0%)	95 (17.7%)	69 (12.8%)	100 (18.6%)	75 (13.9%)
MV	150 (27.9%)	30	19	8	49	44
LV	258 (47.9%)	131	51	39	25	12
DV	130 (24.2%)	38	25	22	26	19

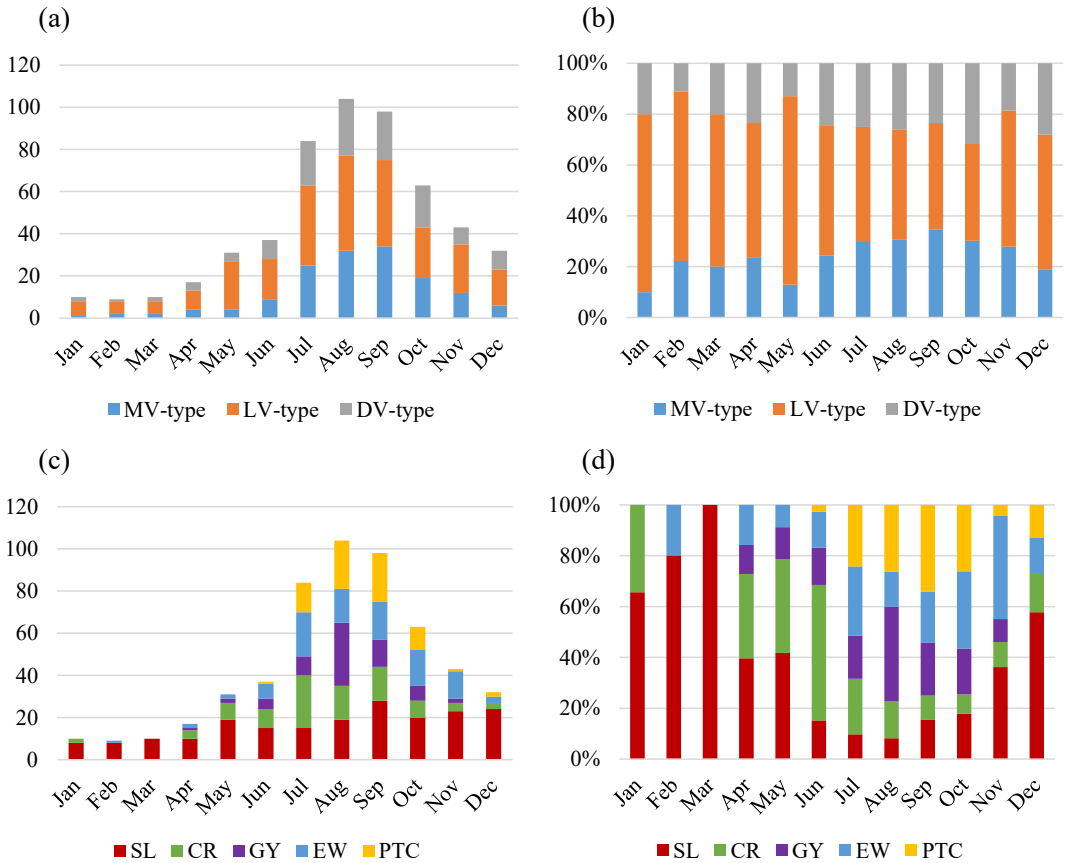

Fig. 4. (a)–(b) Seasonal variation of three archetypes of TC genesis in the WNP for the 20-yr study period from 1999 to 2018. (a) Accumulated number of TC genesis cases per month, and (b) percentages normalized by the monthly total. (c)–(d) Similar to (a)–(b) but for the five flow patterns.

DV-type enhance slightly. Figure 5 shows the regional distribution of TC genesis and the origin of vortex perturbation (the first time when initial vortex can be detected) in three archetypes of TC genesis. The genesis of LV-type occurs preferentially near the equator while the MV- and DV-type occurs more poleward and is scattered over the WNP (Figs. 5a–c). From the average location of each type presented in the subtitle, we can see that the TC genesis locations of all cases are mainly concentrated at 14°N, 135°E (TCs formed east of 165°E or north of 30°N are excluded). The TC genesis locations of MV-type and LV-type occurred on average farther to the north and south, respectively. With respect to the origin of the initial vortex, except for the discrepancy in latitude that has been shown in the TC genesis location, there are also some meridional differences among the three archetypes, i.e., the origins of initial vortex in the MV-type and DV-type are biased to the east and west, respectively (Figs. 5d–f).

Figure 6 gives the time evolution of the composite relative vorticity and divergence averaged within a 2° radius around the vortex center for MV-type, LV-type, and DV-type, respectively. The vortex center is tracked based on filtered relative vorticity averaged between 1000–600 hPa. Data are composited from 5 days before TC genesis and black contours represent the standard deviation. The three archetypes of TC genesis exhibit distinct differences in vorticity enhancement in the center area. The maximum vorticity first appears at the mid and low levels in the MV-type and LV-type, respectively, which is consistent with the archetypes mentioned above and confirms the validity of classification of initial vortexes leading to tropical cyclogenesis in the current study. The DV-type can also be distinguished from the other two types in that it shows a relatively deep vortex structure in the vertical (Fig. 6c). From Figs. 6d–f, the convergence is concentrated near the surface in all types, while the strong convergence (greater than 0.8×10^{-5} s^{-1})

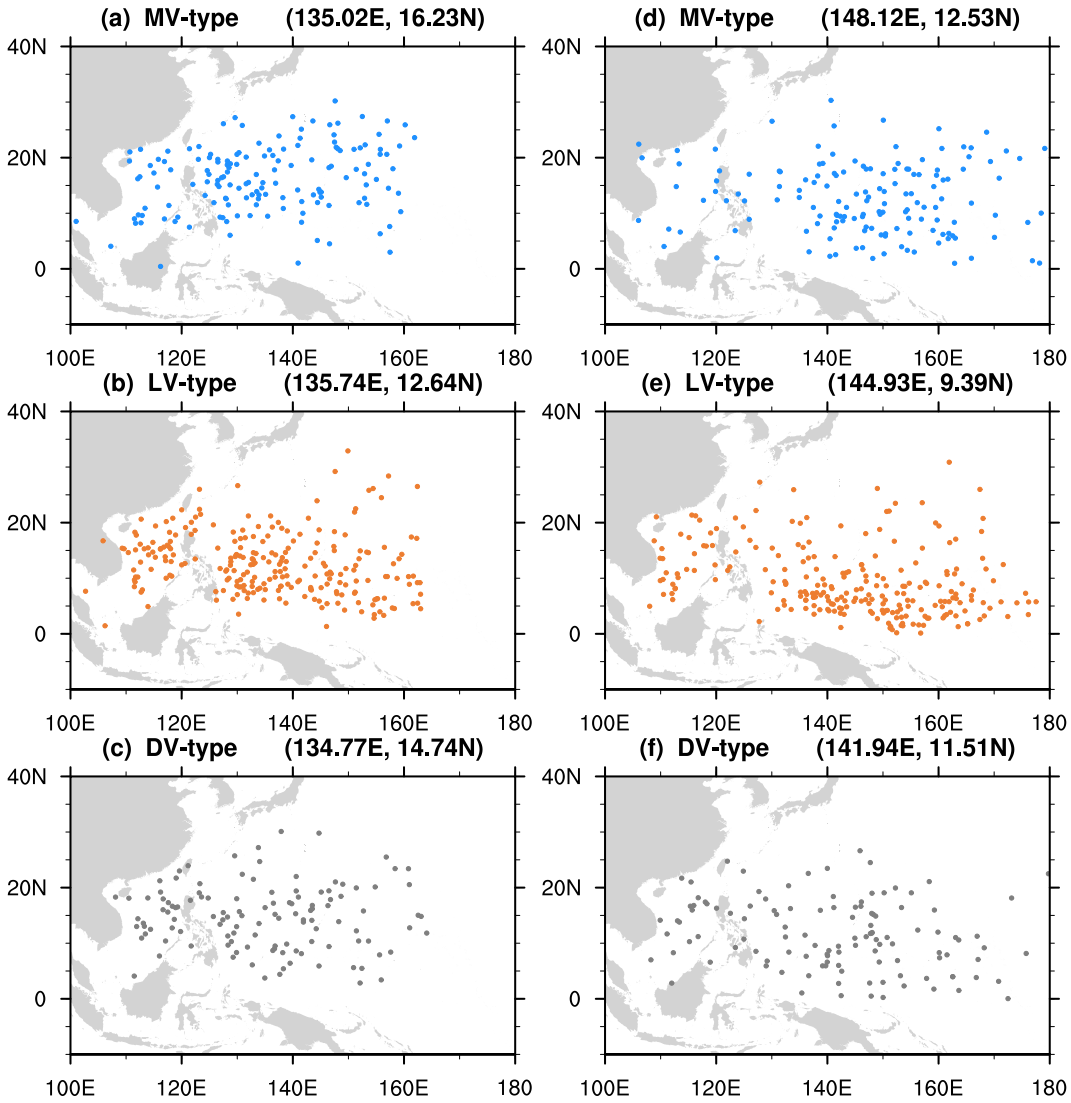

Fig. 5. Genesis distribution of (a) MV-type, (b) LV-type, and (c) DV-type. (d)–(f) Similar to (a)–(c) but for the origin of vortex perturbation (the first time when initial vortex can be detected). The longitude and latitude in the subtitle present the average location for three archetypes of TC genesis.

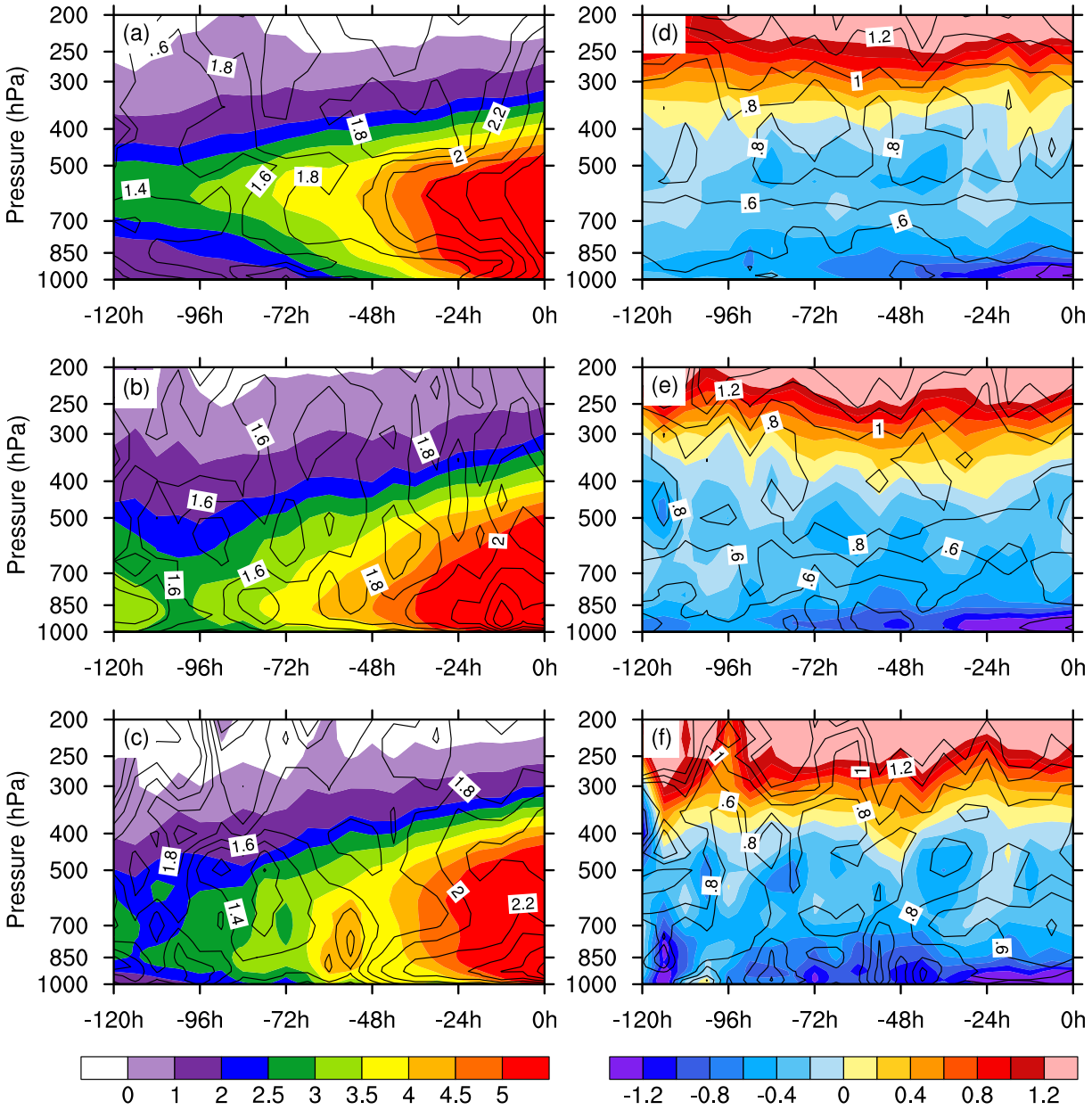

Fig. 6. Time-pressure diagram of composite vertical relative vorticity (shading; units: 10^{-5} s^{-1}) and standard deviation (contours; units: 10^{-5} s^{-1}) averaged within a 2° radius around the vortex center in (a) MV-type, (b) LV-type, and (c) DV-type. (d)–(f) Similar to (a)–(c) but for the horizontal divergence. The vortex center is tracked on the basis of filtered relative vorticity averaged between 1000–600 hPa.

first appears in LV about 72 hours before tropical cyclogenesis, and the convergence in the mid-troposphere is more obvious in DV-type. This will be discussed further in section 3.3.

Figure 7 similarly illustrates the time evolution of composite relative humidity and temperature perturbation in the pre-TC stage. The temperature perturbation is defined as the deviation of the temperature from the environmental average. The increase of moisture content is apparent in all archetypes of TC genesis, especially at 600 hPa. There is a tendency for drying before tropical cyclogenesis, which may correlate with the warm core structure during TC development as well as the environmental intrusion at the same time. The overall environmental moisture condition in the MV-type is drier compared with other two types (Fig. 7a–c). From Figs. 7d–f, the temperature is higher than that of the surrounding environment, especially in the upper troposphere. The warm core develops 5 days before genesis and extends downwards with time from 48 h prior to tropical cyclogenesis. The temperature perturbation in the MV-type is a little bit weaker than that in the other two types (Fig. 7d).

3.2. *The large-scale environmental circulations of three archetypes of TC genesis*

To interpret and verify the differences of TC genesis type in the WNP and the North Atlantic and eastern Pacific,

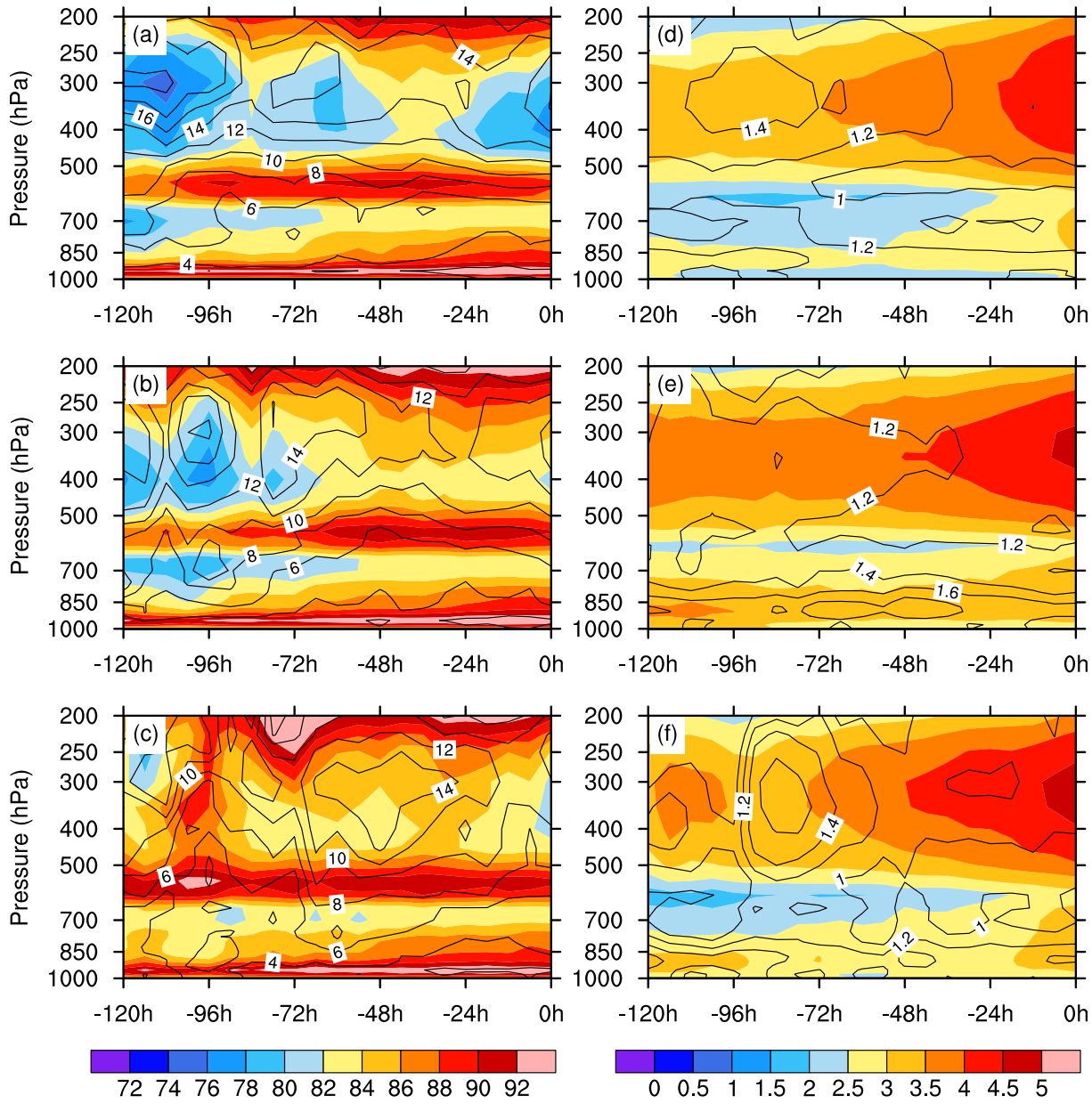

Fig. 7. As in Fig. 6, but for (a)–(c) the relative humidity (units: %), and (d)–(f) the temperature perturbation (units: K). The temperature perturbation is derived by removing the background temperature.

the previously discussed objective detection method was employed following YI13 to categorize the large-scale environmental circulations into five patterns. Table 1 shows the number and percentage of five large-scale flow patterns over the WNP in the period from 1999 to 2018: SL (199 cases, or 37.0%), EW (100 cases, or 18.6%), CR (95 cases, or 17.7%), PTC (75 cases, or 13.9%), and GY (69 cases, or 12.8%). Figures 4c–d displayed the seasonal variation in the proportion of different flow patterns, from which we can see that the tropical cyclogenesis events associated with the SL, CR, and EW occur throughout the year. The percentage of the SL is particularly high in winter due to the existence of westerly or southwesterly winds over the WNP near the equator. The occurrence of GY and PTC cases increases in summer and autumn, respectively, which can be explained by the following considerations. The monsoon gyres tend to be stronger over the WNP in summer, thus the GY flow pattern may be organized more frequently. Moreover, due to the multiple tropical cyclone events and the increase in the number of TCs from summer to autumn, the opportunity for preparing the PTC flow pattern enhances accordingly.

These five flow patterns increase significantly in typhoon seasons, which must have a certain impact on TC activity. To examine the relationship between these large-scale flow patterns and the three archetypes of TC genesis, we categorize the initial vortexes leading to tropical cyclogenesis in the five large-scale background flow patterns. From Table 2 and Fig. 8, we can see that the LV-type dominates in SL, CR, and GY (higher than 50%), while the MV-type is more frequent in PTC and EW. The DV-type happens in

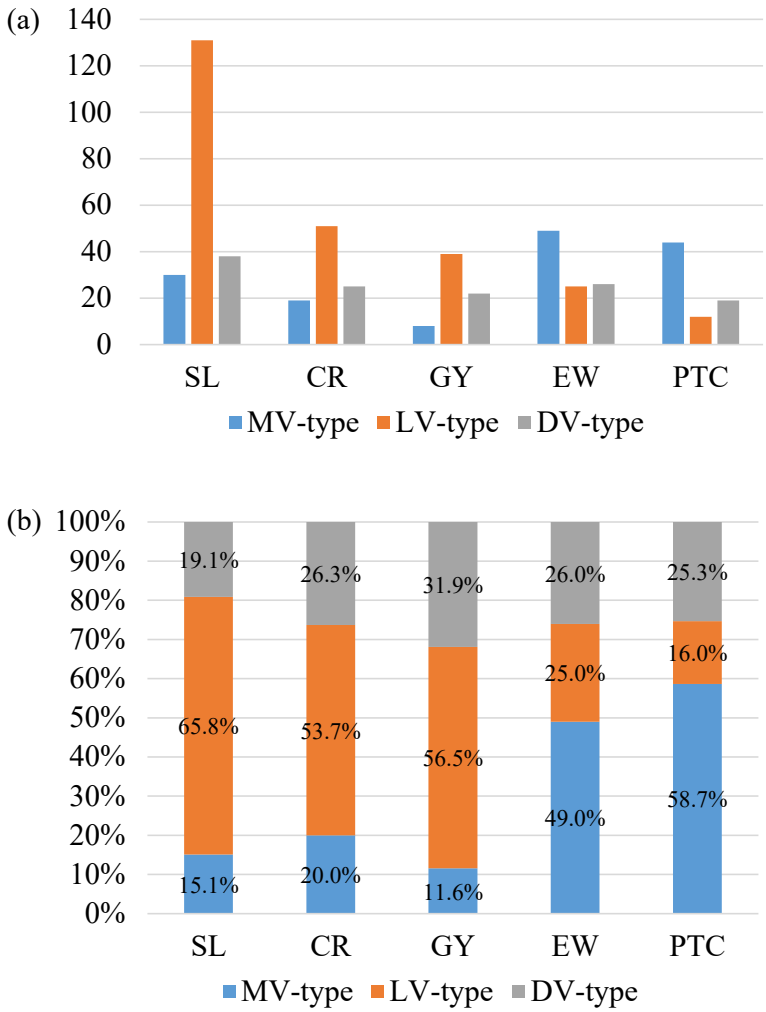

Fig. 8. (a) Accumulated number of archetypes of TC genesis in different large-scale background flow patterns. (b) Similar to (a) but for percentages normalized by total number in each flow pattern.

all flow patterns uniformly. Obviously, the type of initial vortex leading to tropical cyclogenesis is closely related to the environmental flow patterns. This is consistent with the findings from Fu et al. (2007) that the contraction of the disturbances and convergence from the large-scale circulation is a possible mechanism contributing to TC genesis.

The relationship between the three archetypes of TC genesis and the large-scale circulation is much clearer in Fig. 9, which compares the tracking longevity of the low- and mid-level vorticity precursors of TCs in the five large-scale background flow patterns. The tracking longevity is defined as the time from initial vortexes in the low- or mid-levels that can be detected to the TC genesis time. The red dashed line indicates when the tracking longevity is the same at 1000 hPa and 600 hPa. From Fig. 9a, we can see that the longest vorticity precursor of TCs can be tracked for 12 days prior to tropical cyclogenesis, while there are tropical cyclogenesis events without obvious vortex precursors before TC formation (the tracking longevity is zero at both the low- and mid-levels). Consistent with the statistical results, i.e., LV-type dominates among three archetypes of TC genesis, more TCs can be tracked for longer time in the lower troposphere. Among different environmental flow patterns, this situation is much clearer for SL, CR, and GY. These three patterns are closely related to the low-pressure trough with prominent shear, convergence, or cyclonic circulation in the lower troposphere, thus the low-level disturbances will develop relatively earlier.

In the cases of PTC and EW, more TCs can be tracked for a longer time at 600 hPa (Figs. 9b–f). The definitive relationship between EW and PTC is consistent with YI13 that PTC can possibly create and transfer vorticity in the environment and favors the evolution of TCs from the disturbance of the easterly wave, so MV-type dominates in both these patterns. The EW pattern is a synoptic-scale wave within the trade wind system and the maximum amplitude of wave in the easterlies appears approximately at 700 hPa (RH99). As for the PTC pattern, it was illustrated as the consequence of the train of vortices left after the preexisting TC in the southeastward direction through energy dispersion, leading to a

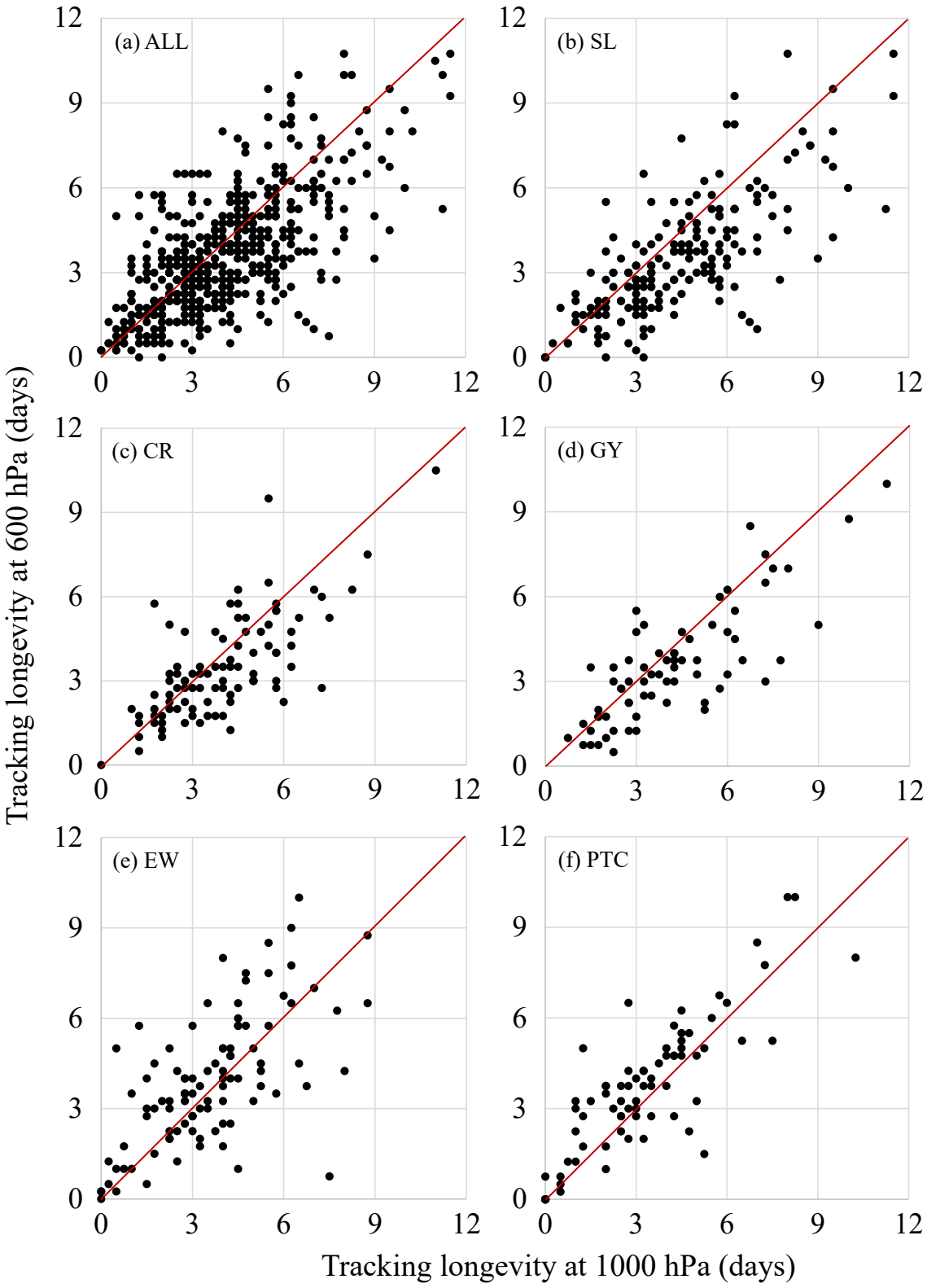

Fig. 9. Scatter diagrams of the tracking longevity at 1000 hPa versus tracking longevity at 600 hPa (days) in different large-scale background flow patterns. The red dashed line indicates when the tracking longevity is the same at 1000 hPa and 600 hPa.

sequence of developing cyclones (Carr III and Elsberry, 1995; McDonald, 1998). Holland (1995) suggested that energy dispersion, phase locked processes, as well as confluence first occur and are most pronounced in the middle troposphere at around 700 hPa. Corresponding to the maximum amplitude of each flow pattern, it is not difficult to interpret

the close relationship between the archetypes of TC genesis and the large-scale flow patterns. The environmental circulation provides favorable environment for the vortexes and disturbances to develop faster at the corresponding level.

Figure 3 showed the origin of three archetypes of TC genesis in the five large-scale flow patterns, and the composite large-scale circulation at the time when TC perturbations first appear. We can see that the geographic distribution of initial vortexes has obvious regional characteristics among different flow patterns. The SL- and CR-TCs (hereafter, SL-TC, CR-TC, and similar terms indicate a TC that formed in SL, CR, or other large-scale flow patterns) occur preferentially equatorward, in keeping with the break of ITCZ and the monsoon trough (Figs. 3b–c). This is reasonable since the SL- and CR-TCs happen at the northern and eastern edge of the monsoon westerly winds, respectively. Compared with SL- and CR-TCs, GY-TCs appear poleward and westward, and the cyclonic circulation is obvious (Fig. 3d, it is much clearer at the TC genesis time, not shown). The EW-TCs can be tracked much farther eastwards from the central Pacific, where broad easterly flow prevails (Fig. 3e). The large-scale circulation of PTC is quite similar to that of the GY pattern (Fig. 3f). From the three archetypes of TC genesis in the five large-scale flow patterns, we can still see that the LV-type dominates in SL, CR, and GY, and the MV-type dominates in PTC and EW, but the regional distribution of initial vortex does not show any significant difference (Figs. 3b–f).

3.3. *The genesis efficiency of the three mesoscale vortexes*

From Fig. 9a, we can see that some vorticity precursors of TCs can be tracked for a very long time while some can only be tracked for a very short time before TC genesis. From comparing the tracking longevity of the vortex system, tropical cyclogenesis efficiency in different types of initial vortexes and flow patterns were investigated. The tracking longevity is defined by the time from when both vortexes in the low- and mid-levels can be detected to the TC genesis time (this is relatively straightfoward for different types of initial vortexes). Long tracking time indicates low efficiency of TC genesis, whereas short time equates to high efficiency. Here, the genesis efficiency differs from TC genesis productivity in Zhao et al. (2018), who denoted the percentage of TC clusters that develop into TCs for specific periods and areas of interest. Figure 10 presents the percentage of tracking longevity in the MV-type, LV-type, and DV-type events. The tracking longevity has a peak at approximately 2–3 days, and more than half of the total TC genesis cases can be tracked within 4 days. In tracking longevity less than 4 days, MV-type is fewer and in tracking longevity between 4 to 5 days, MV-type is extremely high, which may indicate the tropical cyclogenesis efficiency is not that high in MV-type. Meanwhile, the difference between LV- and DV-type is not that significant. There are several cases with tracking longevity longer than 7 days, which mainly result from either insufficient ocean thermal energy in winter and spring, lack of significant planetary vorticity, topographic blocking effects, competition between tropical disturbances, and/or unfavorable moisture conditions. The average tracking longevity of all TC cases is 71.1 h, which implies that on average, the vortex structure can be detected and tracked 3 days before tropical cyclogenesis in the WNP. This is also the reason why we chose the averaged 850-hPa wind field at 66 and 72 h before the TC genesis time when calculating the "contribution scores" from large-scale background flow patterns.

Without considering the cases with tracking longevity longer than 7 days, the average tracking longevity in MV-type, LV-type, and DV-type genesis is ~75.8, 71.2, and 65.6 hours, respectively. The frequencies of TC genesis with

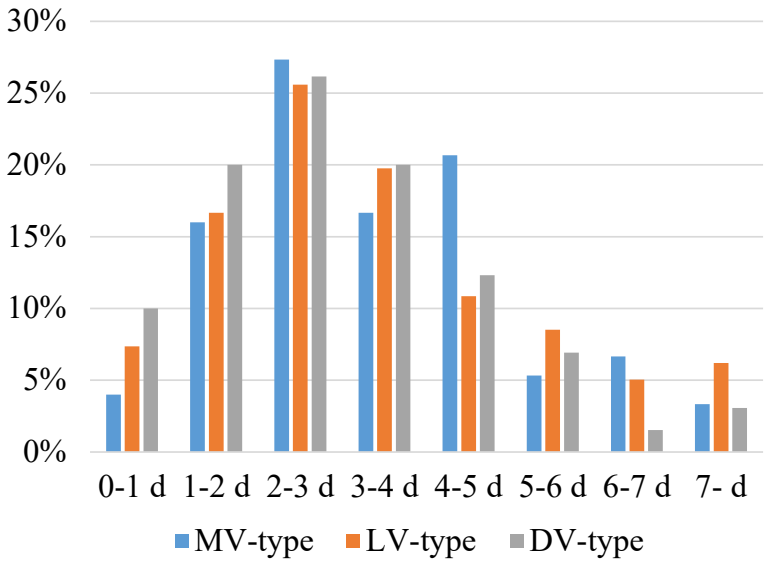

Fig. 10. Percentage of tracking longevity (days) in different archetypes of TC genesis: MV-type (blue), LV-type (orange), and DV-type (gray).

different tracking duration and the corresponding second-order regression for three archetypes of TC genesis are shown in Fig. 11. Regression can reduce the influence of minimum and maximum on the average duration and the axis of the fitting function (μ) represents the median number, which is sometimes more convincing. We could take both average and median into account to better understand the TC genesis efficiency of different archetypes. From Fig. 11, we can see that the axes of symmetry of μ displayed in the upper right corner are 74.2, 70.7, and 64.9 hours for MV-type, LV-type, and DV-type, respectively. These results all indicate that the genesis efficiency is highest in DV, and compared with MV, LV usually takes a shorter time to upgrade to a TC. This is consistent with Ge et al. (2013) that a bottom

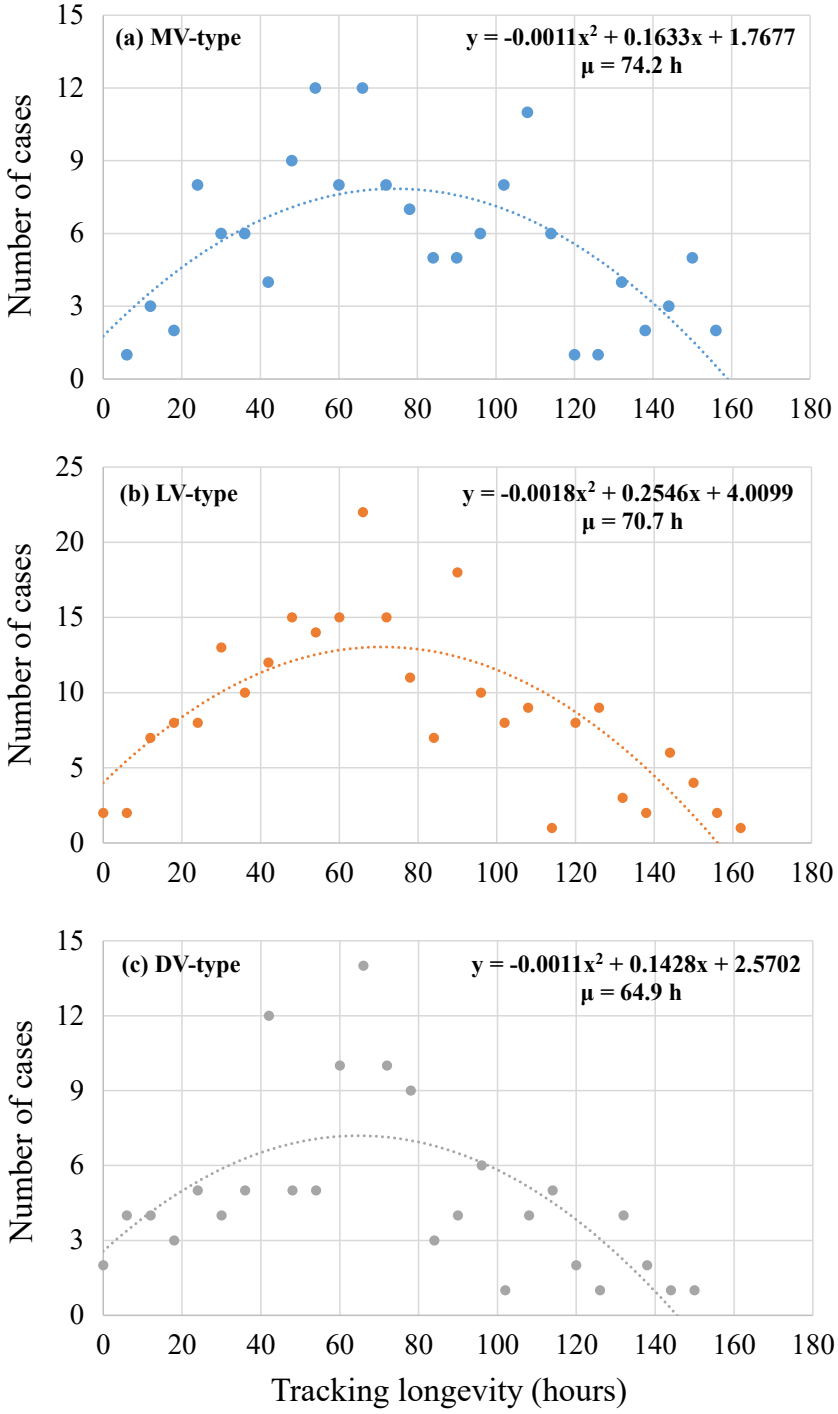

Fig. 11. Scatter diagrams of the tracking longevity of vortexes (hours) in (a) MV-type, (b) LV-type, and (c) DV-type. The curve and μ value in each diagram are the second-order regression and axis of symmetry, respectively. Tracking longevity of cases longer than 7 days are ignored.

vortex has higher genesis efficiency than a mid-level vortex, a result of a study in which a set of idealized numerical simulations with different initial vortex vertical profiles was used.

The composite divergence fields show significant convergence near the surface in all types but there are also some subtle differences (Figs. 6d–f). Strong convergence in the low-levels first appears in LV-type, and convergence in the mid-troposphere is more obvious before tropical cyclogenesis in DV-type (Figs. 6e–f). What's more, the composite relative humidity in the MV-type is slightly lower compared with LV and DV (Figs. 7a–c). Table 3 gives the average convergence, relative humidity, and some other synoptic conditions of TC genesis among the three types of TC genesis events. The relative humidity and vorticity in the lower- and mid-troposphere, 850-hPa convergence, vertical wind shear, and convective available potential energy (CAPE) shown in Table 3 are averaged within a 5° radius of the TC precursor center from 72 h before genesis. The vertical wind shear is defined as the difference in horizontal winds between the 850- and 200-hPa levels. In Table 3, we can see that the mid-level humidity and large-scale convergence at 850 hPa show great differences in MV and LV, with a 5% level of significance. Relatively wet conditions and stronger convergence in LV compared with the MV can explain why the former usually generates and intensifies faster to a tropical cyclone. In MV-type, the surface cyclonic circulation is relatively weak (Fig. 6a) and less conducive to the air-sea interaction and boundary-layer convergence of water vapor and convective development. Besides, the appearance of a surface cyclonic vortex with sufficient amplitude is the sign of TC formation (RH99; Tory et al., 2006a). Therefore, it seems that the LV should be more beneficial to tropical cyclogenesis.

With relatively moist conditions and significant strong convergence (Table 3), TCs develop the fastest in DV, which indicates that the upright vortex structure and relevant internal dynamics may play a critical role in tropical cyclogenesis. During the TC genesis, the high-level vorticity is also enhanced at the same time along with the increase of low- and mid-level vorticity. From the composite relative vorticity of the TC-precursor in the three types of TC genesis (Figs. 6a–c), we can see that the intensification rate of the vorticity in the upper troposphere is in accordance with the tropical cyclogenesis efficiency, i.e., fastest in DV-type and slowest in MV-type. This implies that the genesis efficiency is partly determined by the vertical vortex structure. This is consistent with idealized simulations in Peng and Fang (2021) in which the intensification rate of a shallow vortex is smaller than a relatively deep vortex and the TC takes a longer time to reach a state of slantwise moist neutrality. For a deep vortex, unstable low-level stratification and rapid strengthening of the mid-to-upper level vortex will favor deep convection bursts.

The averaged tracking longevity was calculated for five large-scale background flow patterns associated with tropical cyclogenesis, resulting in: 72.84, 67.98, 69.75, 70.68, and 72.34 hours in the SL, CR, GY, EW, and PTC patterns, respectively. Additionally, the median values in the second-order regression are 72.9, 63.5, 70.6, 69.0, and 72.1 hours, respectively (Fig. 12). The difference in the genesis efficiency among these flow patterns is not significant. Figure 13 shows the percentage of tracking duration in different background flow patterns by classifying them into periods less than and more than 3 days. CR-TCs have a comparably higher genesis efficiency than those in the other flow patterns, which is in accordance with Fudeyasu and Yoshida (2018) that CR-TCs have the highest rates of occurrence of rapid intensification.

To clarify why TCs form and intensify fastest under the influence of the CR pattern, the same TC genesis environmental factors were averaged within a 5° radius of the TC precursor center among five background flow patterns. Table 4 shows that the highest genesis efficiency of CR-TCs is mainly ascribed to favorable moist conditions especially in the mid-troposphere. The average relative humidity of all cases is 76.61% at 500 hPa, and it is a little bit higher (80.08%) in the CR pattern, with a 5% level of significance. It is worth mentioning that there is no difference in the genesis efficiency among the other flow patterns, but all environmental parameters of the EW-TCs show significant differences exceeding 95% confidence level. From Table 4, we can see that EW-TCs exhibit unfavorable environmental characteristics, such as low relative humidity, weak low-level convergence, and cyclonic circulation. The latter may be correlated

Table 3. Statistical summary of atmospheric environmental physical parameters associated with three archetypes of TC genesis averaged within 5° radius of the pre-TC center from 72 h before genesis. Bold characters indicate significant differences exceeding 95% confidence level with a *t* test.

	ALL	MV	LV	DV
1000–500-hPa average RH (%)	82.576	**81.605**	82.969	83.044
850-hPa RH (%)	83.152	82.583	83.369	83.455
500-hPa RH (%)	76.609	**74.843**	77.378	77.331
850-hPa convergence (10^5 s^{-1})	0.316	**0.276**	0.328	**0.346**
1000–600-hPa vorticity (10^5 s^{-1})	1.738	1.734	1.728	1.766
850-hPa vorticity (10^5 s^{-1})	1.937	1.861	1.981	1.945
Vertical wind shear (m s^{-1})	8.296	8.215	8.347	8.294
CAPE (J kg^{-1})	638.921	639.455	637.666	641.092

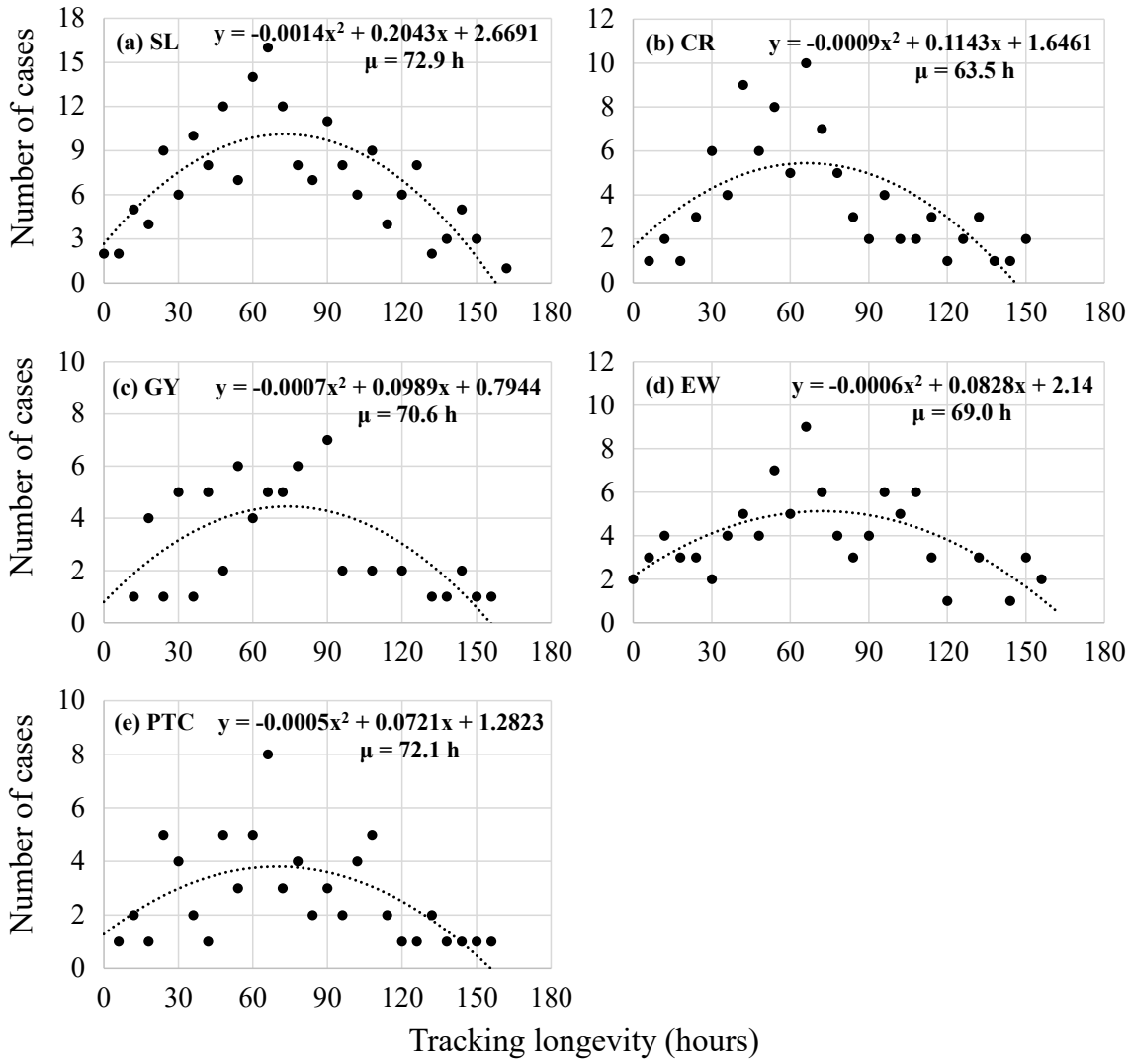

Fig. 12. As in Fig. 11 but for tracking longevity (hours) in different large-scale background flow patterns.

with the convection characteristics in the EW-TCs formations, in which the convection depth is shallower than that in other monsoon-related formations and convection occurs closer to the center (Lee et al., 2008). However, with weaker vertical wind shear and larger CAPE, the genesis efficiency of EW-TCs shows no apparent discrepancy with other categories except CR-TCs.

4. Discussion

It is worth mentioning that the results presented in this work are derived from the ERA5 reanalysis data and thus it is necessary to examine whether the results are robust using different reanalysis datasets. Tables 5 and 6 are the statistical summary of archetypes of TC genesis and five large-scale flow patterns in the NWP derived from the 1-degree ERA-Interim dataset from 1979 to 2018 and the 1-degree NCEP FNL dataset from 1999 to 2018, respectively. Comparing Tables 2, 5, and 6, we can see that the numbers of the different genesis types and background circulations derived from the different datasets are different. However, the percentages of the three genesis types and the five background circulations are equivalent. It is worth noting that the percentage of five large-scale flow patterns associated with tropical cyclogenesis in the WNP is comparable with many previous results (e.g., Ritchie and Holland, 1999; Wu et al., 2013; Yoshida and Ishikawa, 2013; Zong and Wu, 2015). It is found that the categorization obtained in this work is like that presented in the previous works (Table 1).

To evaluate the sensitivity of the findings in this work to the best-track dataset, the archetypes of TC genesis were tested with different kinds of data sources from JTWC, CMA, and JMA (Table 7). There are respectively 538, 527, and 455 TCs in the best-track datasets of JTWC, CMA, and JMA over the WNP basin from 1999 to 2018 (TCs formed east of 165°E or north of 30°N are excluded). TC records from CMA are quite close to those from JTWC, which are much greater in number than that of JMA. Some tropical depressions are ignored in the JMA dataset. From Table 7, we can see that the total numbers of the TC genesis types

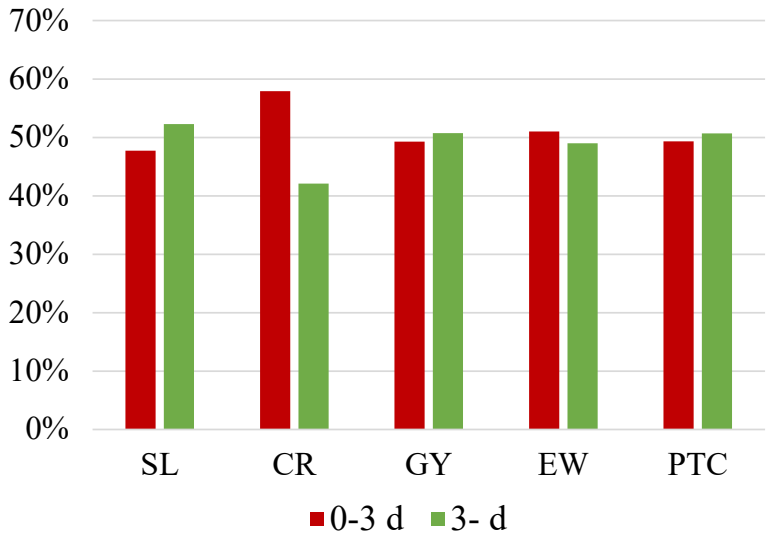

Fig. 13. Percentage of tracking duration (less than or more than 3 days) in different large-scale background flow patterns. Tracking longevity of cases longer than 7 days are ignored.

Table 4. Similar to Table 3 except for five large-scale flow patterns.

	ALL	SL	CR	GY	EW	PTC
1000–500-hPa average RH (%)	82.574	82.836	**83.730**	83.179	**81.141**	82.005
850-hPa RH (%)	83.154	83.318	83.959	83.527	**82.249**	82.728
500-hPa RH (%)	76.606	77.377	**80.080**	**79.050**	**72.149**	**74.605**
850-hPa convergence (10^5 s^{-1})	0.316	**0.331**	0.328	0.307	**0.293**	0.304
1000–600-hPa vorticity (10^5 s^{-1})	1.739	1.735	1.852	**2.163**	**1.319**	1.774
850-hPa vorticity (10^5 s^{-1})	1.938	1.968	2.086	**2.256**	**1.554**	1.911
Vertical wind shear (m s^{-1})	8.295	8.496	8.670	8.735	**6.850**	8.780
CAPE (J kg^{-1})	638.92	625.37	642.62	637.28	**670.12**	630.03

Table 5. Similar to Table 2 except for the ERA-Interim dataset from 1979 to 2018.

	ALL	SL	CR	GY	EW	PTC
ALL	1026	398 (38.79%)	188 (18.32%)	98 (9.55%)	189 (18.42%)	153 (14.91%)
MV	307 (29.92%)	46	26	33	103	99
LV	455 (44.35%)	228	117	47	51	12
DV	264 (25.73%)	124	45	18	35	42

Table 6. Similar to Table 2 except for the NCEP FNL dataset.

	ALL	SL	CR	GY	EW	PTC
ALL	524	195 (37.2%)	92 (17.6%)	69 (13.2%)	98 (18.7%)	70 (13.4%)
MV	147 (28.1%)	32	17	8	50	40
LV	249 (47.5%)	125	52	39	23	10
DV	128 (24.4%)	38	23	22	25	20

derived from different data sources are different; however, the percentages of the three genesis types are equivalent. Noteworthy is that the genesis locations are verified to be quite close among three datasets.

In addition to the sensitivities of the results to the reanalysis datasets and best-track data, the possible influences of the tracking method on the results presented in this work are also evaluated. We conducted the vortex tracking with TempestExtremes (Ullrich et al., 2021) in the typhoon seasons in 2017 and 2018. The result shows that, of 64 TCs in 2017 and 2018, 19 (14) TCs originated from MV-type (DV-type) and 31 TCs from LV-type, which is comparable to that

Table 7. Statistical summary of archetypes of TC genesis in the NWP from 1999 to 2018 compared with different kinds of data sources from JTWC, CMA, and JMA.

	JTWC	CMA	JMA
ALL	538	527	455
MV	154 (28.6%)	151 (28.7%)	133 (29.2%)
LV	249 (46.3%)	244 (46.3%)	216 (47.5%)
DV	135 (25.1%)	132 (25.0%)	106 (23.3%)

derived from the TRACK from Hodges, i.e., 19 (12) TCs originated from MV-type (DV-type) and 33 TCs from LV-type. This result indicates that the TRACK from Hodges works well in the detection of the vorticity perturbations in tropical cyclogenesis. Some previous studies (e.g., Pinto et al., 2013, 2016) have also compared TRACK with other systems before and verified the solid performance of TRACK from Hodges.

Finally, the sensitivity of tracker was also tested with a different vorticity threshold of 5×10^{-4} s^{-1}. The classification results as well as TC genesis efficiency were quite close to the current study. The average tracking longevity in MV-type, LV-type, and DV-type genesis is ~62.5, 60.24, and 57.79 hours, respectively. The threshold of vorticity in our manuscript is determined by the area-averaged vorticity, which includes all vorticity centers that formed south of 50°N is 1.5×10^{-5} s^{-1} at 900 hPa for 48 h or more could be identified and tracked (Galarneau et al., 2015).

5. Concluding remarks

By using the ECMWF ERA5 reanalysis data at 0.25° resolution and the TC best track from JTWC, this study investigates the statistical characteristics of the initial mesoscale vortexes leading to tropical cyclogenesis events with a 20-yr analysis set from 1999 to 2018 of totally 538 TCs over the WNP. It is found that the mesoscale vortexes that result in the formation of TCs in WNP can be categorized into three types: the mid-level vortex (MV), the low-level vortex (LV), and the relatively deep vortex with notable vorticity in both the lower and middle troposphere (DV) by tracking the vortex centers in the low- and mid-levels, respectively. The tropical cyclogenesis events related to different archetypes occur in all months and do not exhibit obvious seasonal variabilities. The regional distribution of TC genesis and the origin of vortex perturbation show that the TC genesis locations of MV-type and LV-type occurred on average farther to the north and south, respectively and the origins of initial vortex in the MV-type and DV-type are biased to the east and west, respectively. The composite analysis of the time evolution of the vortex structure suggests that the maximum vorticity first appears at the mid- and low-levels in MV and LV, respectively, while the DV-type can also be distinguished from the other two types by a relatively deep vortex structure in the vertical. The convergence is concentrated near the surface in all types, while the strong convergence first appears in LV-type, and the convergence in the mid-troposphere is more obvious in DV-type.

A distinction from that which occurs in the North Atlantic and eastern Pacific regions, most vortexes that cause TC formation in the WNP first appeared in the lower troposphere (47.9%) or developed at the same time in the low- and mid-levels (24.2%), and only 27.9% of tropical cyclones (TCs) developed first in the mid-troposphere. These differences might be ascribed to the active monsoon systems in the WNP being present all year round. The large-scale background flow pattern of the monsoon trough makes it easier for the low-level disturbance to develop much faster in WNP.

The environmental circulation related to each type of tropical cyclogenesis over the WNP was determined from classifying the large-scale background flows of TC formation into five patterns, i.e., monsoon shear line (SL), monsoon confluence region (CR), monsoon gyre (GY), easterly wave (EW), and wave energy dispersion of preexisting TC (PTC) via calculating the modified "contribution scores", first proposed by YI13. The results indicate that the TC genesis events associated with LV mostly occurred in the SL, CR, and GY patterns, whereas those associated with MV prefer to happen in the EW and PTC patterns, which corresponds to the maximum amplitude of each flow pattern. The DV-type happens in all flow patterns uniformly.

Upon comparing the tracking longevity of the original vortex in the pre-genesis stage, it is found that there are some differences in the TC genesis efficiency among different types of initial vortexes and the large-scale flow patterns. The generation efficiency is the highest in DV-type, which is ascribed to the nearly upright vortex structure and deep convergence 120 h before genesis. TC generates and intensifies faster in LV-type than MV-type owing to relatively moister conditions and stronger convergence correlated with the surface cyclonic vortex, which is related to greater air-sea interaction and boundary-layer convergence. Among flow patterns, the CR-TCs usually take a shorter time to upgrade to a tropical cyclone compared with other flow patterns, which is mainly due to favorable moist conditions, especially in the middle troposphere.

This work investigates the original vortexes leading to tropical cyclogenesis events and the associated environmental background flow in WNP. The findings are statistically significant for improving our understanding of tropical cyclogenesis. The tracking duration of the vortex may have something to do with the predictable scale. However, it is worth mentioning that although the tropical cyclogenesis event can be traced back to an original MV, LV, or DV, the low- and mid-level vortexes usually develop or strengthen sequentially during the formation of a TC due to the intermittent outbreaks of deep convection (Wu and Fang, 2019). How the original mesoscale vortex works with the convection to affect the vorticity fields in the lower to middle troposphere and finally lead to the formation of a TC is one of the most important issues in the tropical cyclogenesis deserving in-depth study.

Acknowledgements. This work was supported in part by the Nature Science Foundation of China under Grant Nos. 41875046, 42175004, National Key Research and Development Program of China under Grant No. 2017YFC1501601, Shanghai "Science and Technology Innovation Action Plan" Yangtze River Delta Science and Technology Innovation Community Field Project Grant 21002410200. Computing is performed at the High Performance Computing Center in Nanjing University.

REFERENCES

Bister, M., and K. A. Emanuel, 1997: The genesis of Hurricane Guillermo: TEXMEX analyses and a modeling study. *Mon. Wea. Rev.*, **125**, 2662–2682, https://doi.org/10.1175/1520-0493(1997)125<2662:TGOHGT>2.0.CO;2.

Briegel, L. M., and W. M. Frank, 1997: Large-scale influences on tropical cyclogenesis in the western North Pacific. *Mon. Wea. Rev.*, **125**, 1397–1413, https://doi.org/10.1175/1520-0493(1997)125<1397:LSIOTC>2.0.CO;2.

Carr III, L. E., and R. L. Elsberry, 1995: Monsoonal interactions leading to sudden tropical cyclone track changes. *Mon. Wea. Rev.*, **123**, 265–290, https://doi.org/10.1175/1520-0493(1995)123<0265:MILTST>2.0.CO;2.

Chu, J. H., C. R. Sampson, A. S. Levine, and E. Fukada, 2002: The Joint Typhoon Warning Center tropical cyclone best-tracks, 1945-2000. Rep. NRL/MR/7540-02-16, 22 pp. [Available online from http://www.usno.navy.mil/NOOC/nmfc-ph/RSS/jtwc/best_tracks/TC_bt_report.html]

Davis, C. A., and L. F. Bosart, 2004: The TT problem: Forecasting the tropical transition of cyclones. *Bull. Amer. Meteor. Soc.*, **85**, 1657–1662, https://doi.org/10.1175/BAMS-85-11-1657.

DeMaria, M., J. A. Knaff, and B. H. Connell, 2001: A tropical cyclone genesis parameter for the tropical Atlantic. *Wea. Forecasting*, **16**, 219–233, https://doi.org/10.1175/1520-0434(2001)016<0219:ATCGPF>2.0.CO;2.

Duchon, C. E., 1979: Lanczos filtering in one and two dimensions. *J. Appl. Meteor.*, **18**, 1016–1022, https://doi.org/10.1175/1520-0450(1979)018<1016:LFIOAT>2.0.CO;2.

Dunkerton, T. J., M. T. Montgomery, and Z. Wang, 2009: Tropical cyclogenesis in a tropical wave critical layer: Easterly waves. *Atmospheric Chemistry and Physics*, **9**, 5587–5646, https://doi.org/10.5194/ACP-9-5587-2009.

Emanuel, K. A., 1994: *Atmospheric Convection*. Oxford University Press, 580 pp.

Fang, J., and F. Q. Zhang, 2010: Initial development and genesis of hurricane Dolly (2008). *J. Atmos. Sci.*, **67**, 655–672, https://doi.org/10.1175/2009JAS3115.1.

Fu, B., T. Li, M. S. Peng, and F. Z. Weng, 2007: Analysis of tropical cyclogenesis in the Western North Pacific for 2000 and 2001,. *Wea. Forecasting*, **22**, 763–780, https://doi.org/10.1175/WAF1013.1.

Fudeyasu, H., and R. Yoshida, 2018: Western North Pacific tropical cyclone characteristics stratified by genesis environment. *Mon. Wea. Rev.*, **146**, 435–446, https://doi.org/10.1175/MWR-D-17-0110.1.

Galarneau, T. J. Jr., R. McTaggart-Cowan, L. F. Bosart, and C. A. Davis, 2015: Development of north Atlantic tropical disturbances near upper-level potential vorticity streamers. *J. Atmos. Sci.*, **72**, 572–597, https://doi.org/10.1175/JAS-D-14-0106.1.

Ge, X. Y., T. M. Li, and M. S. Peng, 2013: Tropical cyclone genesis efficiency: Mid-level versus bottom vortex. *Journal of Tropical Meteorology*, **19**, 197–213, https://doi.org/10.16555/j.1006-8775.2013.03.001.

Gray, W. M., 1968: Global view of the origin of tropical disturbances and storms. *Mon. Wea. Rev.*, **96**, 669–700, https://doi.org/10.1175/1520-0493(1968)096<0669:GVOTOO>2.0.CO;2.

Guo, C. R., and Q. H. Zhang, 2012: A study of the role of mesoscale vortex merging in the genesis of Typhoon Durian (2001). *Acta Meteorologica Sinica*, **70**, 1–14, https://doi.org/10.11676/qxxb2012.001. (in Chinese with English abstract)

Harr, P. A., R. L. Elsberry, and J. C. L. Chan, 1996: Transformation of a large monsoon depression to a tropical storm during TCM-93,. *Mon. Wea. Rev.*, **124**, 2625–2643, https://doi.org/10.1175/1520-0493(1996)124<2625:TOALMD>2.0.CO;2.

Hendricks, E. A., M. T. Montgomery, and C. A. Davis, 2004: The role of "vortical" hot towers in the formation of Tropical Cyclone Diana (1984). *J. Atmos. Sci.*, **61**, 1209–1232, https://doi.org/10.1175/1520-0469(2004)061<1209:TROVHT>2.0.CO;2.

Hodges, K. I., 1994: A general method for tracking analysis and its application to meteorological data. *Mon. Wea. Rev.*, **122**, 2573–2586, https://doi.org/10.1175/1520-0493(1994)122<2573:AGMFTA>2.0.CO;2.

Hodges, K. I., 1995: Feature tracking on the unit sphere. *Mon. Wea. Rev.*, **123**, 3458–3465, https://doi.org/10.1175/1520-0493(1995)123<3458:FTOTUS>2.0.CO;2.

Hodges, K. I., 1999: Adaptive constraints for feature tracking. *Mon. Wea. Rev.*, **127**, 1362–1373, https://doi.org/10.1175/1520-0493(1999)127<1362:ACFFT>2.0.CO;2.

Hodges, K., A. Cobb, and P. L. Vidale, 2017: How well are tropical cyclones represented in reanalysis datasets. *J. Climate*, **30**, 5243–5264, https://doi.org/10.1175/JCLI-D-16-0557.1.

Holland, G. J., 1995: Scale interaction in the western Pacific monsoon. *Meteorol. Atmos. Phys.*, **56**, 57–79, https://doi.org/10.1007/BF01022521.

Komaromi, W. A., 2013: An investigation of composite dropsonde profiles for developing and nondeveloping tropical waves during the 2010 PREDICT Field Campaign. *J. Atmos. Sci.*, **70**, 542–558, https://doi.org/10.1175/JAS-D-12-052.1.

Kurihara, Y., M. A. Bender, and R. J. Ross, 1993: An initialization scheme of hurricane models by vortex specification. *Mon. Wea. Rev.*, **121**, 2030–2045, https://doi.org/10.1175/1520-0493(1993)121<2030:AISOHM>2.0.CO;2.

Kurihara, Y., M. A. Bender, R. E. Tuleya, and R. J. Ross, 1995: Improvements in the GFDL hurricane prediction system. *Mon. Wea. Rev.*, **123**, 2791–2801, https://doi.org/10.1175/1520-0493(1995)123<2791:IITGHP>2.0.CO;2.

Lander, M. A., 1994: Description of a monsoon gyre and its effects on the tropical cyclones in the western North Pacific during August 1991,. *Wea. Forecasting*, **9**, 640–654, https://doi.org/10.1175/1520-0434(1994)009<0640:DOAMGA>2.0.CO;2.

Lee, C.-S., K. K. W. Cheung, J. S. N. Hui, and R. L. Elsberry, 2008: Mesoscale features associated with tropical cyclone formations in the western North Pacific. *Mon. Wea. Rev.*, **136**, 2006–2022, https://doi.org/10.1175/2007MWR2267.1.

McDonald, N. R., 1998: The decay of cyclonic eddies by Rossby wave radiation. *J. Fluid Mech.*, **361**, 237–252, https://doi.org/10.1017/S0022112098008696.

Möller, J. D., and M. T. Montgomery, 2000: Tropical cyclone evolution via potential vorticity anomalies in a three-dimensional

balance model. *J. Atmos. Sci.*, **57**, 3366–3387, https://doi.org/10.1175/1520-0469(2000)057<3366:TCEVPV>2.0.CO;2.

Montgomery, M. T., and J. Enagonio, 1998: Tropical cyclogenesis via convectively forced vortex Rossby waves in a three-dimensional quasigeostrophic model. *J. Atmos. Sci.*, **55**, 3176–3207, https://doi.org/10.1175/1520-0469(1998)055<3176:TCVCFV>2.0.CO;2.

Montgomery, M. T., M. E. Nicholls, T. A. Cram, and A. B. Saunders, 2006: A vortical hot tower route to tropical cyclogenesis. *J. Atmos. Sci.*, **63**, 355–386, https://doi.org/10.1175/JAS3604.1.

Peng, K., and J. Fang, 2021: Effect of the initial vortex vertical structure on early development of an axisymmetric tropical cyclone. *J. Geophys. Res.*, **126**, e2020JD033697, https://doi.org/10.1029/2020JD033697.

Pinto, J. G., N. Bellenbaum, M. K. Karremann, and P. M. Della-Marta, 2013: Serial clustering of extratropical cyclones over the North Atlantic and Europe under recent and future climate conditions. *J. Geophys. Res.*, **118**, 12 476–12 485, https://doi.org/10.1002/2013JD020564.

Pinto, J. G., S. Ulbrich, T. Economou, D. B. Stephenson, M. K. Karremann, and L. C. Shaffrey, 2016: Robustness of serial clustering of extratropical cyclones to the choice of tracking method. *Tellus A: Dynamic Meteorology and Oceanography*, **68**(1), 32204, https://doi.org/10.3402/tellusa.v68.32204.

Raymond, D. J., S. L. Sessions, and C. López Carrillo, 2011: Thermodynamics of tropical cyclogenesis in the northwest Pacific. *J. Geophys. Res.*, **116**, D18101, https://doi.org/10.1029/2011JD015624.

Raymond, D. J., S. Gjorgjievska, S. Sessions, and Ž. Fuchs, 2014: Tropical cyclogenesis and mid-level vorticity. *Australian Meteorological and Oceanographic Journal*, **64**, 11–25, https://doi.org/10.22499/2.6401.003.

Ritchie, E. A., and G. J. Holland, 1997: Scale interactions during the formation of Typhoon Irving. *Mon. Wea. Rev.*, **125**, 1377–1396, https://doi.org/10.1175/1520-0493(1997)125<1377:SIDTFO>2.0.CO;2.

Ritchie, E. A., and G. J. Holland, 1999: Large-scale patterns associated with tropical cyclogenesis in the western Pacific. *Mon. Wea. Rev.*, **127**, 2027–2043, https://doi.org/10.1175/1520-0493(1999)127<2027:LSPAWT>2.0.CO;2.

Simpson, J., E. Ritchie, G. J. Holland, J. Halverson, and S. Stewart, 1997: Mesoscale interactions in tropical cyclone genesis. *Mon. Wea. Rev.*, **125**, 2643–2661, https://doi.org/10.1175/1520-0493(1997)125<2643:MIITCG>2.0.CO;2.

Tory, K. J., M. T. Montgomery, and N. E. Davidson, 2006a: Prediction and diagnosis of tropical cyclone formation in an NWP system. Part I: The critical role of vortex enhancement in deep convection. *J. Atmos. Sci.*, **63**, 3077–3090, https://doi.org/10.1175/JAS3764.1.

Tory, K. J., M. T. Montgomery, N. E. Davidson, and J. D. Kepert, 2006b: Prediction and diagnosis of tropical cyclone formation in an NWP system. Part II: A diagnosis of tropical cyclone Chris formation. *J. Atmos. Sci.*, **63**, 3091–3113, https://doi.org/10.1175/JAS3765.1.

Ullrich, P. A., C. M. Zarzycki, E. E. McClenny, M. C. Pinheiro, A. M. Stansfield, and K. A. Reed, 2021: TempestExtremes v2.1: A community framework for feature detection, tracking, and analysis in large datasets. *Geoscientific Model Development*, **14**, 5023–5048, https://doi.org/10.5194/gmd-14-5023-2021.

Wu, L. G., H. J. Zong, and J. Liang, 2013: Observational analysis of tropical cyclone formation associated with monsoon gyres. *J. Atmos. Sci.*, **70**, 1023–1034, https://doi.org/10.1175/JAS-D-12-0117.1.

Wu, S. L., and J. Fang, 2019: The evolution and role of midtropospheric cyclonic vortex in the formation of Super Typhoon Nepartak (2016). *J. Geophys. Res.*, **124**, 9277–9298, https://doi.org/10.1029/2019JD030631.

Yoshida, R., and H. Ishikawa, 2013: Environmental factors contributing to tropical cyclone genesis over the western North Pacific. *Mon. Wea. Rev.*, **141**, 451–467, https://doi.org/10.1175/MWR-D-11-00309.1.

Zawislak, J., and E. J. Zipser, 2014: A Multisatellite investigation of the convective properties of developing and nondeveloping tropical disturbances. *Mon. Wea. Rev.*, **142**, 4624–4645, https://doi.org/10.1175/MWR-D-14-00028.1.

Zhang, W. L., X. P. Cui, and J. X. Dong, 2010: The role of middle tropospheric mesoscale convective vortex in the genesis of typhoon Durian (2001)-Diagnostic analysis of simulated data. *Chinese Journal of Atmospheric Sciences*, **34**, 45–57, https://doi.org/10.3878/j.issn.1006-9895.2010.01.05. (in Chinese with English abstract)

Zhang, W. L., X. P. Cui, and J. X. Dong, 2021: Characteristics and mechanism of vertical coupling in the genesis of tropical cyclone Durian (2001). *Science China Earth Sciences*, **64**, 440–457, https://doi.org/10.1007/s11430-019-9681-x.

Zhao, H. K., S. H. Chen, P. J. Klotzbach, and G. B. Raga, 2018: Impact of the extended boreal summer intraseasonal oscillation on western North Pacific tropical cloud cluster genesis productivity. *J. Climate*, **31**, 9175–9191, https://doi.org/10.1175/JCLI-D-18-0113.1.

Zong, H. J., and L. G. Wu, 2015: Re-examination of tropical cyclone formation in monsoon troughs over the Western North Pacific. *Adv. Atmos. Sci.*, **32**, 924–934, https://doi.org/10.1007/s00376-014-4115-2.